Development of a Magnetic Intra-Uterine Manipulator

***S Doll*[a], *C Scheffer*[b] *and G du Toit*[c]**

Received 1 February 2013 and accepted 13 September 2013

This paper introduces the concept of a novel magnetic intra-uterine manipulator, intended to overcome conventional medical devices' shortcomings, and enabling non-invasive uterine manipulation during surgery. However, analyses have shown that the magnetic manipulator is unable to compete in terms of the range of motion of the existing devices. A limited anterior sagittal rotation range of 60° was observed in a magnetic manipulator compared to a range of 140° for conventional devices. Despite these limitations, use of a magnetic manipulator could eliminate the need for an additional medical assistant during surgery; it is also reusable and thus also more economical. The second goal of the research was to investigate which type of setup would be most successful in effective uterine manipulation. Through concept analysis, a cart-on-arch system was deemed most effective. To lift an effective load of 1 N over an air gap of 150 mm, rare-earth N38 neodymium (NdFeBr) magnets showed the most promise as magnetic actuators for the manipulator. Finite Element Analysis (FEA) simulations of the magnetic set-up were validated experimentally and produced an acceptable Mean Absolute Error (MAE) of 0.15 N.

Keywords – Laparoscopic instrumentation, minimally invasive surgery, uterine manipulation, surgical robotics

[a] Biomedical Engineering Research Group
Dept of Mechanical and Mechatronic Engineering,
Stellenbosch University.

[b] Biomedical Engineering Research Group
Dept of Mechanical and Mechatronic Engineering,
Stellenbosch University.
E-mail: cscheffer@sun.ac.za

[c] Dept Obstetrics and Gynaecology
Stellenbosch University.

Nomenclature

A	Area of the magnetic pole
B	Flux density
B_r	Remnant flux density
B_{xcyl}	Flux density at distance x
F	Magnetic force
F_x	Magnetic force at distance x
L	Length of magnet
R	Radius of cylinder
x	Length of air gap

1. Introduction

A hysterectomy is a procedure in which either part of or the entire uterus is removed from the female reproductive tract. About 1 000 000 hysterectomies are performed annually, worldwide[1]. To put that number into perspective, roughly 900 000 cardiac surgeries are performed worldwide within the same time frame[2]. Nowadays, an ever-increasing number of these hysterectomies are being performed laparoscopically. This type of surgery is a minimally invasive procedure, where small incisions are made in the abdominal wall. Ports are then inserted into these incisions through which the surgeon has access to the abdomen. The surgery is performed with tools inserted through the ports and viewed on a Liquid Crystal Display (LCD) screen via an abdominal camera. Laparoscopies limit external scarring, reduce patient recovery time, reduce tissue trauma in the patient, and are generally less invasive than the conventional norm, namely abdominal hysterectomies. Unfortunately, a laparoscopic hysterectomy is much more complicated than an abdominal hysterectomy, where the uterus can easily be visualised and manipulated through the incision in the abdomen. This means that more intricate tools are required in the already expansive array of laparoscopic surgical equipment.

The critical factor in laparoscopic surgery is the ability to manipulate the uterus as extensively and as easily as possible to gain access to surrounding tissue that needs to be dissected from the uterus. A variety of uterine manipulators have been developed for this purpose; most of them cover essentially the same design of a cervically inserted, manually controlled actuator. These designs generally work well, but require the presence of an additional medical assistant to operate the manipulator. A user-friendly and less expensive system that can be controlled by only one surgeon would thus be of great benefit to surgeons and patients alike.

This paper presents the development and critical evaluation of a uterine manipulator that is actuated magnetically (refer to figure 1) using an internal permanent magnet (IPM) and external permanent magnet (EPM).

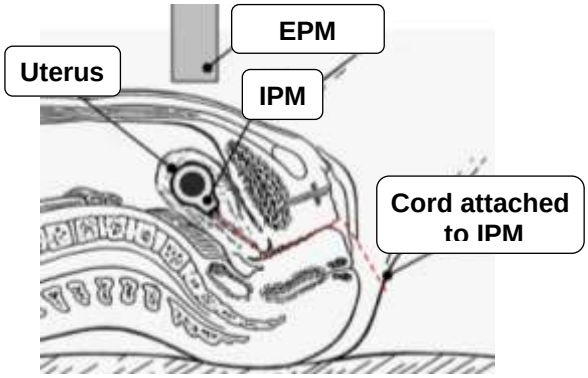

Figure 1: Position of IPM inside the uterus (adapted from[3])

Existing uterine manipulators offer a rather crude, albeit functional, solution for uterine manipulation. Most manipulators have a very similar design, with a flexible tip, an extension shaft and the manipulator handle, as depicted in figure 2. Use of a manipulator during surgery requires insertion of the manipulator through the vagina into the cervical canal and lodging the tip in the uterus itself. The manipulator remains in the vaginal and cervical canal for the duration of the surgery. In addition to the discomfort caused by the hysterectomy, the patient often experiences tissue trauma inflicted unintentionally by trying to position the manipulator correctly in the cervix. Due to the large number of hysterectomies performed worldwide, there is a significant need to ensure the safety and well-being of the patients undergoing these surgeries.

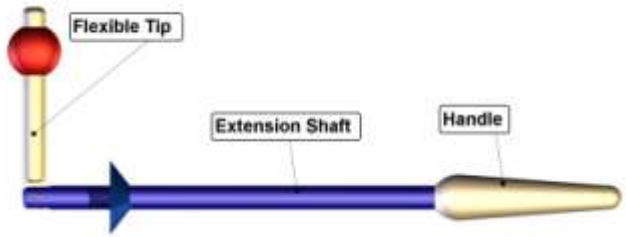

Figure 2: Example of a mechanical uterine manipulator

Existing uterine manipulators are rather expensive; they range from $390 to $2 500 (US$). Many of these are not reusable either, adding to the already high surgery costs of $6 000 to $15 000, according to Sculpher *et al.*[4]. This makes the prospect of using a simple grasper or forceps for manipulation more attractive, which in turn has the disadvantage of taking up an extra laparoscopic port. Finally, most uterine manipulators require an extra assistant during surgery to operate the manipulator. This limits space in the theatre and again increases the total cost of the operation.

Research into the development of a magnetic intra-uterine manipulator therefore offers a promising concept for a surgical tool that is easy to use, patient- and surgeon-friendly, and makes effective use of the limited theatre space.

2. Design Criteria

The primary requirement for this design was that the magnets be capable of lifting a load of at least 1 N over a distance of 150 mm. The load requirement of 1 N was determined from the average weight of a uterus of 80 g (0.785 N), as published by Martini *et al.*[5]. The air gap of 150 mm was derived analytically from the minimum distance possible between the external and the internal magnets. This air gap takes into consideration the distance between the patient's uterus and the external abdominal surface, as well as the minimum distance of the eternal magnet from the patient's abdominal surface of 20 mm, as per Ciuti *et al.*[6]. Furthermore, the magnetic influence of human tissue was assumed to be the same as that of air (figure 3) in order to simplify modelling. Consequently, the gap between the two magnets was modelled as an air space. Lastly, it was important to limit the speed of the device's movement to avoid damaging organs or interfering with surgical tools during the surgery. In order to meet these criteria, the selection of suitable magnets was a key aspect of the design. There are a variety of magnet types and configurations to consider, including magnet shapes, different types of permanent magnets, electromagnets, permanent/electro-magnet hybrids and even different magnet housing configurations. The three major design features were: the manipulator frame, the IPM and the EPM.

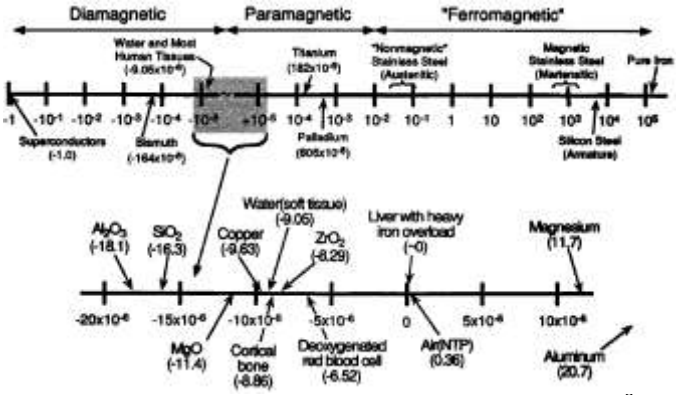

Figure 3: Susceptibility spectrum for known materials[6]

2.1 Manipulator frame: cart-on-arch design

After an extensive literature research on existing magnetic devices which interact with the human body in a surgical environment, a cart-on-arch system was chosen as the most appropriate frame for the manipulator. The concept is depicted in figure 4.

For the setup to be a successful candidate for future deployment it had to be a simple and elegant solution. The arch system was designed to be no wider than 130 mm to avoid obstructing the surgeon in the already cluttered operating theatre. It was also designed to be placed directly over the uterus in the abdominal section, leaving access to all the laparoscopic ports in the upper abdominal area open. In addition, the device was designed to be very easy to

move and control. However, the range of motion that the system is able to manipulate the uterus is slightly limited compared to existing mechanical manipulators.

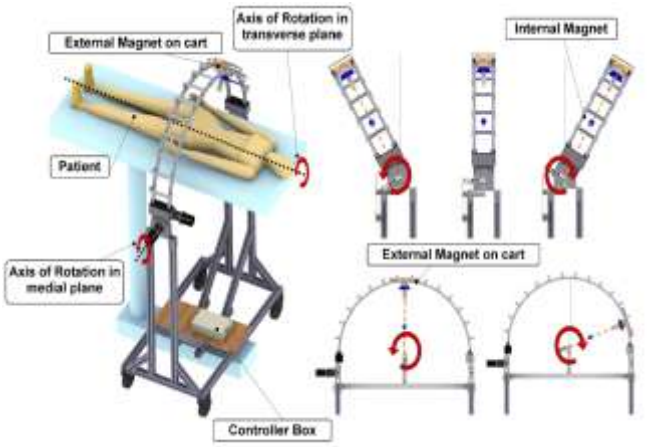

Figure 4: Cart-on-arch concept

Compared to the systems in table 1, the arch design achieves a good range of motion for lateral manipulation of the uterus with a possible range of 140°, whereas anteversion and retroversion are only possible over a range of 60°. Unfortunately, this latter key design aspect is poorer than that of a mechanical manipulator owing to space limitations at the operating table. Any further rotation of the arch might cause dangerous interference with the surgeon. To make up for the lack of rotation, the arch design is very easy to manipulate: four buttons (two for each motor) are used to easily control the direction of rotation.

Table 1: Comparison of uterine manipulators to a magnetic uterine manipulator, adapted from[7]

Manipulator	Movement			Reusable	Maintenance	Independent Movement	Ease of Assembly	Cost
	Anteversion / Retroversion	Lateral	Elevation					
Clermont-Ferrand	140°	120°	140°	Yes	✓✓✓	✓✓✓✓	✓	±$250
Hald	120°	90°	140°	Yes	✓✓	✓✓✓	✓	±$4500
Endopath	120°	90°	140°	No	✓✓	✓	✓✓	N/A
RUMI with Koh-cup	140°	90°	140°	Partially	✓✓✓	✗	✓	±$200
Hoecable	90°	140°	140°	Yes	✓	✓✓✓✓	✓✓✓	N/A
Vcare	90°	90°	140°	No	✓✓✓	✗	✓✓✓✓	N/A
TLH-Dr Mangalvikar	120°	90°	140°	Yes	✓✓✓	✓✓	✓✓✓	±$2500
ClearView	170°	120°	140°	No	✓✓	✓✓	✓	N/A
Cohen Cannula	140°	120°	140°	No	✓✓✓	✓	✓✓	±$500

✗ = "Not Applicable", ✓ = "Slightly Applicable", ✓✓ = "Moderately Applicable", ✓✓✓ = "Applicable", ✓✓✓✓ = "Very Applicable"

2.2 Design of the internal permanent magnet and housing

According to a study by Merz *et al.*[8], confirmed by Ellis and Mahadevan[9] and Martini *et al.*[5], the average length and width of the uterus for pre- and postmenopausal women are 7.5 cm and 4.1 cm respectively. As with most uterine manipulators, the cervix has to be dilated to enable insertion.[7] Therefore, the design of the IPM is drastically limited by the space available in the uterus. Unfortunately, the IPM could not be simulated independently from the EPM, as the finite element analysis (FEA) software (MagNET by Infolytica) outputs the force solution as a force balance between the two magnets.

As indicated in figure 5, the magnet will be encased by an ergonomically designed plastic housing with smooth edges for easy insertion. This design offers protection from the risk of infection or irritation due to corrosion of the IPM in the uterus. It also enables the spherical magnet to rotate freely in the housing, maintaining perfect alignment with the external magnetic field and allowing for maximum attraction force between the two magnets. Furthermore, the risk of tissue trauma is eliminated because the magnet housing is unable to rotate as positioned in the uterus. It can also be manufactured from biocompatible material to prevent irritation and eliminate possible allergic reactions to the material.

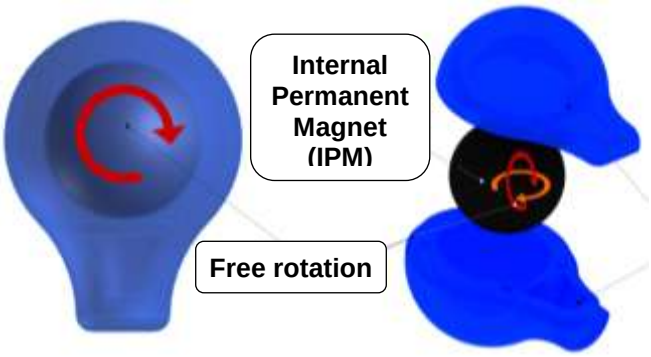

Figure 5: Internal permanent magnet housing and magnet orientations

A spherical N38 grade NdFeBr magnet was chosen for the prototype system. These magnet types exhibit the highest flux densities of rare-earth permanent magnets and are thus the best suited magnet types for this application. With the space available in the uterus, the maximum size spherical magnet available which could be chosen has a 20 mm diameter. The housing of the internal magnet was manufactured by using a rapid prototyping process from SKEG Product Development (Cape Town, South Africa). The wall thickness of the housing was fixed at 3 mm to maintain the structural integrity of the housing in the uterus. The housing was manufactured using FullCure 720 polyethylene material. figure 6 depicts the completed prototypes.

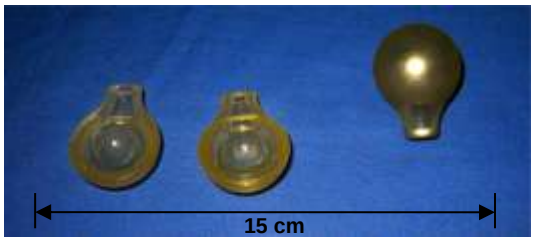

Figure 6: Prototypes of internal magnet housing

2.3 Design of the external permanent magnet

Permanent magnets can be manufactured in various shapes and sizes. Some designs are tailored to achieve maximum contact force, whereas other designs are better suited to attracting a magnetic body over a certain distance. Parker[10] states that to attract a magnetic body over a distance, the goal is to maximize the work (force over distance) of the system. This is done by configuring the magnets to enable deep field pattern projection, which is achieved by positioning the poles of the configuration far apart. This constrains the magnetic cores to cylindrical or cubic shapes where the lengths of the cores are considerably larger than the diameter or the width. Cylindrical cores were chosen as their magnetic flux dispersion is more uniform.

The second part of the process involved the selection of a suitable permanent magnetic material. As with the IPM selection, NdFeBr magnets have the highest remnant flux density, B_r compared to any other material and are thus the obvious choice for a permanent external magnet. Equation 1, used in the magnetic design industry, was applied to estimate the flux density present a certain distance x away from the core[11] (illustrated in figure 7).

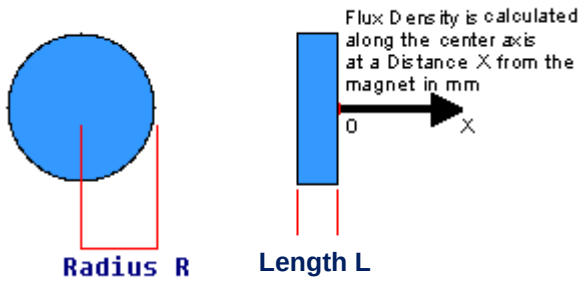

Figure 7: Flux density at a distance from a single rod magnet

Equation 1 calculates the flux density at x for cylindrical magnets:

$$B_{x_{cyl}} = \frac{B_r}{2}\left(\frac{L+x}{\sqrt{R^2+(L+x)^2}} - \frac{x}{\sqrt{R^2+x^2}}\right) \qquad (1)$$

where B_x is the flux density at the distance x, B_r is the remnant flux density at the exit pole of the magnet, R is the radius of the disk and L is its length. The distance away from the pole constrained to the centre axis of the magnets is given by x. figure 8 depicts the flux density over the distance that the external magnet is expected to operate on while the graph insert zooms into the area of interest at a distance of 150–170 mm. As depicted, there is a clear advantage to using a cylindrical magnet over a cubic magnet, since the cylindrical magnet has almost double the flux density at any distance away from the pole. Furthermore, force is directly proportional to the flux density of a magnet meaning that the cylindrical magnet is able to generate a higher pulling force.

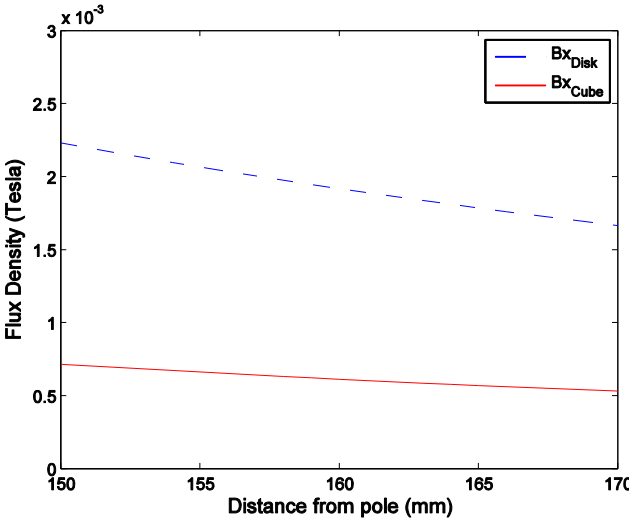

Figure 8: Flux density versus distance

To estimate the force on the magnet at the required distance away from the magnet, the one-dimensional empirical equation 2 was used[11]:

$$F = 0.577B^2A \qquad (2)$$

where F is the pulling force in pounds, B is the flux density at a certain distance from the magnet (calculated from equation 1) in kilogauss (kG) and A is the area of the magnet pole, which can be rewritten as πR^2. As equation 2 is in imperial units, equation 1 has to be converted to imperial units in order to be able to combine the equations. Substituting the value of B from equation 1 into equation 2 and rewriting A as defined above gives:

$$F_x = 0.577\pi R^2 \left(\frac{B_r}{2}\left(\frac{L+x}{\sqrt{R^2+(L+x)^2}} - \frac{x}{\sqrt{R^2+x^2}}\right)\right)^2 \qquad (3)$$

where F_x is the force at a certain distance x away from the magnet which has length L and radius R.

Figure 9 depicts a graphical representation of the above equation over a range of radii and lengths. The distance x was fixed at 170 mm. Interestingly, the force exerted by the magnet increases exponentially with only a minor increase in diameter size at a certain point.

Modelling the force using equation 3 can yield a good estimate of what the magnet dimensions R and L should be to achieve a force of 1 N at a distance of 150 mm away from the pole. Thus, a good initial estimation for these dimensions could be made as a starting point for the FEA. It should be noted that equation 3 assumes that the attracted object on which the force is acting is made from steel. Therefore, the equation contains an intrinsic error if the properties of the attracted material vary greatly from those

of steel, and analysis by means of FEA is essential to arrive at a more accurate solution to the problem. Infolytica's MagNET v.6 was used for the FEA. First, the simulations had to be verified by means of a validation study to ensure the model accuracy and optimal mesh size and solving methods. A N38 NdFeBr magnet with a diameter of 30 mm and a height of 100 mm was chosen as the external magnet, as it was easy to procure. Its high *Br* value meant that it would induce a large attraction force on the spherical magnet, which could be measured experimentally.

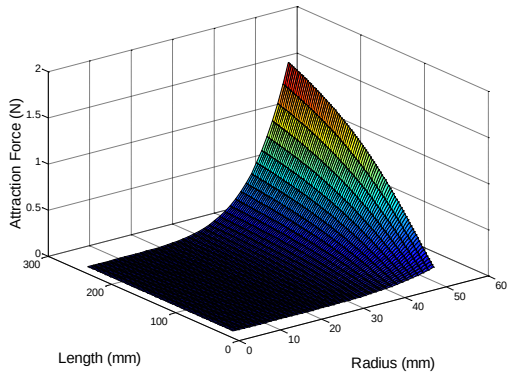

Figure 9: Force as a function of height and radius of a magnet

The problem was solved numerically in MagNET using an axisymmetric model, meaning that only a quarter of the problem had to be modelled. The problem could thus be solved in two instead of three dimensions, reducing computational costs. Figure 10(a) depicts the layout of the design in three dimensions and figure 10(b) depicts the model set-up in the MagNET solver.

The environment meshing was an ongoing process that had to be validated before a judgement on the model's accuracy could be passed. Since the simulation models for this problem consisted only of non-current-carrying elements, MagNET implements the Maxwell stress method to calculate forces on the bodies. This method involves force computations over the layer of air elements that are directly in contact with the body. As a result, this method can lead to error computations in the mesh because the actual geometry of the body is ignored. Therefore, features such as holes and surface imperfections (sharp edges) are not taken into consideration. To measure the degree of error, an error plot was created in MagNET. Such a plot is dimensionless; it only describes the error of the model by measuring discontinuities in the magnetic flux and plotting them as a colour gradient on a scale of zero to one.

For the magnetic system, the mesh size, h-adaption and polynomial order of the solver were refined until the residual error was 0.112, and which was confined to a small region around the top and bottom circumferential edge of the cylinder. The simulation was validated experimentally and the following simulation parameters were set:

- Cylindrical magnet mesh size: 0.3 mm
- Spherical magnet mesh size: 0.3 mm
- Air field mesh size: 0.5 mm
- h-adaption: 25 %, with a tolerance of 0.001 %
- Polynomial order: 4

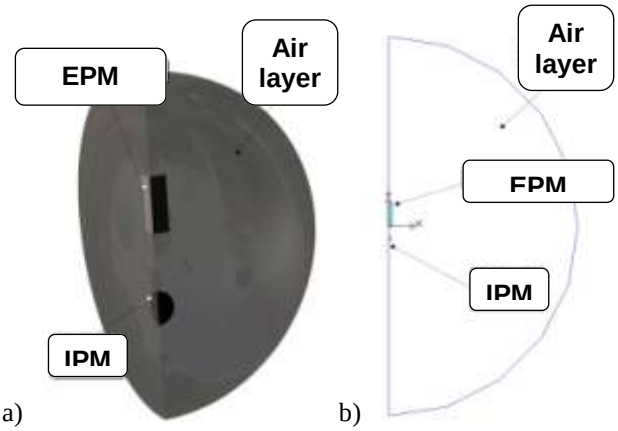

Figure 10: Axisymmetric model description

3. Manipulator Experiments

Two experiments were performed to prove that the magnet design achieved the required attraction force and that the manipulator rotation limits adequately compared to the limits of existing manipulators. The final prototype external magnet had a diameter of 30 mm and a height of 200 mm. This magnet was selected since it is the largest N38 NdFeBr magnet available in South Africa at the time of the research.

A validation study needed to be performed to accurately gauge the simulation performance and accuracy. Figure 11 depicts the set-up of the test rig used to measure the force from the external magnet on the internal magnet. The load cell that was utilised was a high-accuracy HBM PW6CMR/20KG load cell, with a sensitivity of 2.2 mV/V and a maximum measurable load of 20 kg. It was mounted on an adjustable arm (as depicted in the figure) to enable the load cell to always measure the load perpendicular to the bottom surface of the external magnet.

As the arm is always rotated with the movement of the external magnet, the force should always be similar around the circumference of the arch. The internal magnet, encased in its housing, was attached to the load cell via 2 mm thick wire. The load cell was attached to a Spider8 instrument amplifier (HBM, Germany), which was in turn connected to a laptop, via USB, running the data acquisition program Catman®Easy by HBM.

Testing of the force was done in the vertical direction, as depicted in figure 11, to correspond with the simulation data. Furthermore, testing was done over an air-gap ranging from 20 mm to 110 mm, which was increased in increments of 5 mm.

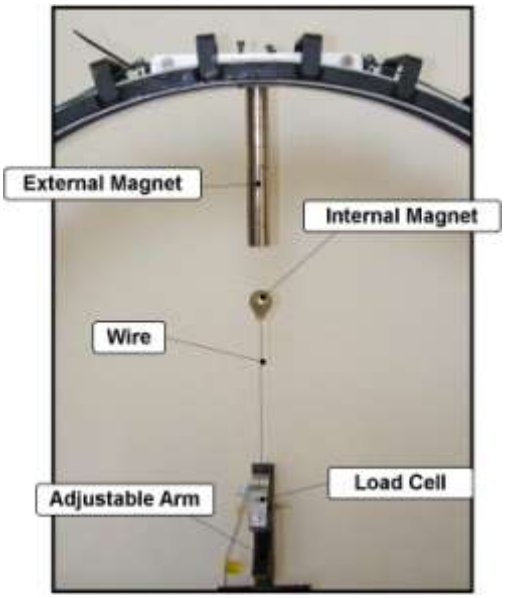

Figure 11: Experimental test setup

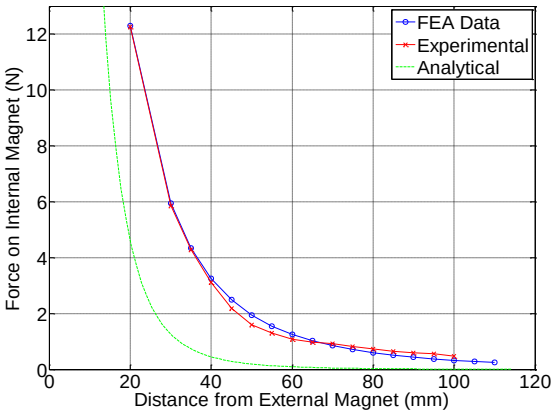

Figure 12: Final magnet prototype (d = 30 mm, h = 200 mm), correlation factor R = 0.9984

As can be seen from figure 12, the analytical calculations of the force using equation 3 are inaccurate and can thus only be used as an initial estimate for the necessary magnet dimensions. The setup was simulated in MagNET according to the parameters fixed in the validation of the magnetic model. It can be seen that the experimental data deviates slightly from the simulation results, especially with larger air-gaps. However, the correlation factor R of the experimental and simulation data is 0.9984. This means that the experimental data agree strongly with the results attained through the simulation. The Mean Absolute Error (MAE) was calculated to be 0.1492 N, which was less than the MAE of the validation model. The error might be attributed to a meshing error or perhaps the influence of the steel arch potentially strengthening the field. Nevertheless, since the simulation results are slightly less than the experimental results the risk of an under-design is minimal.

A final simulation to determine the magnet diameter and the height of a magnet that has the potential to attract the internal magnet with a force of 1 N over a distance of 150 mm was completed. The result was a magnet with a diameter of 110 mm and a height of 200 mm. The resultant design had an attraction force of 1.532 N. This model is expected to be a successful external magnet, but will still have to be verified experimentally.

4. Conclusion

The design of the external permanent magnet was successful for proving the concept of external magnetic intra-uterine manipulation, and compares favourably to existing systems in terms of cost and time effectiveness. It can be reused, operation does not require any extra assistance, it does not need to be assembled and insertion of the internal magnet is simple. Moreover, unlike mechanical designs the device prevents tissue damage to the cervix and vagina, which benefits the patient's well-being. However, several drawbacks were highlighted. The prototype magnetic intra-uterine manipulator had a slightly superior lateral movement range (140°) compared to other commercial systems (90-130°), but its retroversion\anteversion range (60° vs. 90-170°) and elevation (60° vs. 140°) were inferior. Furthermore, while FEA results correlated quite strongly with experimental data the MAE value of 0.1492 suggests that non-negligible errors may occur in experiments with air-gaps approaching the required 150 mm. Care should thus be taken to understand and minimize magnetic interferences and other factors influencing the attraction force during operation. It should also be noted that the analytical equations did not provide an accurate estimation of the required magnet geometry. Even though the largest commercially available magnet was used, it was found from simulations that a magnet diameter approximately four times larger is required to successfully manipulate a uterus in the abdomen.

5. Future work

Several improvements to the proposed design should be investigated. Firstly, the use of electromagnets for the EPM would improve safety by allowing the system to be switched off, although currently available electromagnets may be impractical due to the high current requirements and numerous windings. Another topic that warrants further research is the optimisation of a magnetic shield tailored to deep field generation by changing the geometry or material. Lastly, developing methods to locate the internal magnet from the outside to establish a feedback loop would enable position control of the internal magnet. This would give the surgeon even more control over the position of the uterus.

References

1 *Mettler L, Sammur W and Schollmeyer T*, Hysterectomy for uterine disease in 2010: from past to future, *Clinical*

Medicine Insights: Reproductive Health, 4, 1, 7–22, 2010.

2 *Wijeysundera D, Beattie W, Austin P, Hux J and Laupacis A,* Non-invasive cardiac stress testing before elective major non-cardiac surgery: population based cohort study, *British Medical Journal*, 340: b5526, 2010.

3 *Kavic M and Levinson C,* Prevention and management of laparoendoscopic surgical complications, Society of Laparoendoscopic Surgeons, 1999.

4 *Sculpher M, Manca A, Abbott J, Fountain J, Mason S and Garry R,* Cost effectiveness analysis of laparoscopic hysterectomy compared with standard hysterectomy: results from a randomised trial, *British Medical Journal*, 328:134, 2004.

5 *Martini F, Bartholomew E, Ober W, Garrison C, Welch K and Hutchings R,* Essentials of Anatomy & Physiology, Prentice Hall, 2000.

6 *Ciuti G, Valdastri P, Menciassi A and Dario P,* Robotic magnetic steering and locomotion of capsule endoscope for diagnostic and surgical endoluminal procedures, *Robotica*, 28, 2, 199–207, 2010.

7 *Mettler L and Nikam Y,* A comparative survey of various uterine manipulators used in operative laparoscopy, *Gynecological Surgery*, 3, 4, 239–243, 2006.

8 *Merz E, Miric-Tesanic D, Bahlmann F, Weber G and Wellek S,* Sonographic size of uterus and ovaries in pre- and postmenopausal women, *Ultrasound in Obstetrics & Gynecology*, 7, 1, 38–42, 1996.

9 *Ellis H and Mahadevan V,* Clinical Anatomy: Applied Anatomy for Students and Junior Doctors, 12th Edition, Wiley-Blackwell, 2010.

10 *Parker R,* Advances in Permanent Magnetism, Wiley, 1990.

11 *Australian Magnetic Solutions* *www.magneticsolutions.com.au/magnet-formula.html*, October 2011.